

Role of Diisocyanate Structure on Self-Healing and Anticorrosion Properties of Waterborne Polyurethane Coatings

Changjiang Yu, Martina Salzano de Luna,* Andrea Russo, Ignazio Adamiano, Fabio Scherillo, Zhanhua Wang, Xi Zhang, Hesheng Xia, and Marino Lavorgna

Organic coatings are extensively investigated as possible solution to prevent or at least retard the occurring of corrosion processes on metal surfaces. Their actual breakthrough is still hampered by the risk of barrier properties loss because of local failure of the coating integrity. To address this issue, self-healing coatings, which are intrinsically able to recover from damages upon exposure to external stimuli, are currently gaining increasing attention. Herein, waterborne polyurethanes (PU) are synthesized, and a Diels–Alder adduct is added into the polymeric backbone to endow the material with self-healing functionality. The effect of different diisocyanate in PU synthesis is explored, namely isophorone diisocyanate, 4,4'-dicyclohexylmethane diisocyanate (HMDI), and hexamethylene diisocyanate. The obtained results highlight the key role of the interactions among soft and hard segments in ultimately defining the coating performances. Actually, the combination of Fourier transform infrared spectroscopy, atomic force microscopy and X-ray diffraction analysis reveals that the HMDI-based PU have showed the best balance in terms of H-bonding strength among hard segments and crystallinity degree in the soft ones. This allows to reach a good compromise in terms of mechanical resistance, anticorrosion properties, and self-healing ability.

safety.^[1] Benefiting from continuous innovation in the field of material science and engineering, organic coatings have been successfully developed and exploited for a multitude of applications,^[2–6] and in the last years they stepped up as reliable yet affordable protective solutions to face corrosion problems.^[7] In case of accidental damages, scratches, or aging, the coating integrity is lost, causing the exposure of the underlying metal surface to the surrounding environment. This represents one of the main limiting factors for the real exploitation of protective coatings in highly demanding fields, such as cultural heritage preservation. In the last years, two strategies have been mainly pursued to address this issue. On the one hand, direct incorporation of corrosion inhibitors into coating formulations^[8,9] or their encapsulation into suitable nanocarriers^[10,11] have been proved to provide protection of the metal substrate even when the coating barrier properties fail. On the

other hand, the polymer matrix itself can be engineered to exhibit self-healing ability, by which the coating can self-repair possible damages in order to avoid interaction of the metal with aggressive species in the environment.^[12–16]

In the field of self-healing coatings, polyurethanes (PU) are gaining increasingly attention, thanks to the extremely rich and diversified chemistry behind their synthesis, which provides a versatile toolbox for the development of multifunctional materials.^[17–19] As an example, Liu et al. recently proposed a polyurethane-based material having biomimetic protective features and endowed with self-healing ability.^[20] In addition, in the modern environmentally conscious society, water-based formulations are typically preferred to solvent-based ones.^[21] In this regard, Langer and co-workers highlighted the crucial role of precursor composition and reaction conditions in ultimately determining the physicochemical properties of waterborne polyurethanes, which have to be properly selected in order to fit the targeted application.^[22] The effect of the macrodiol-to-diol ratio, the type of diol chain extender, the structure and molecular weight of the macrodiol, and NCO/OH molar ratio represent just some examples of materials-related parameters that have been systematically investigated and prove to have a key role in determining the functional properties of polyurethane-based


1. Introduction

Metal corrosion is an interfacial degradation process that causes huge economic losses and also poses serious threats to human

C. Yu, Dr. Z. Wang, Prof. X. Zhang, Prof. H. Xia
State Key Laboratory of Polymer Materials Engineering
Polymer Research Institute of Sichuan University
Chengdu 610065, China

Dr. M. Salzano de Luna, A. Russo, I. Adamiano, Dr. F. Scherillo
Department of Chemical, Materials and Production Engineering
University of Naples Federico II
P.le Tecchio 80, Naples 80125, Italy
E-mail: martina.salzanoluna@unina.it

Dr. M. Salzano de Luna, Dr. M. Lavorgna
Institute for Polymers, Composites and Biomaterials
National Research Council of Italy
P.le E. Fermi 1, Portici 80055, Italy

 The ORCID identification number(s) for the author(s) of this article can be found under <https://doi.org/10.1002/admi.202100117>.

© 2021 The Authors. Advanced Materials Interfaces published by Wiley-VCH GmbH. This is an open access article under the terms of the Creative Commons Attribution License, which permits use, distribution and reproduction in any medium, provided the original work is properly cited.

DOI: 10.1002/admi.202100117

systems.^[23–26] Focusing on coatings for corrosion protection, Li et al. addressed the influence of the proportion of polyester and polyether polyols in soft segments on the coating properties.^[27] The goal of the present work is to provide a further insight into the structure–property relationships of waterborne polyurethanes. In particular, intrinsically self-healing polyurethanes with a Diels–Alder (DA) adduct^[28–31] in the main chain were synthesized by using different diisocyanates and the same polyether polyol and chain extender. Their performances were deeply investigated, aiming at elucidating the best formulation for the development of self-healing protective coatings. Our results highlight that the simple tailoring of the polyurethane chemistry allows to combine high barrier properties that are needed to ensure anticorrosion properties, with sufficient molecular mobility, which is instead a prerequisite for efficient mending ability.

2. Results and Discussion

2.1. Phase Morphology and Self-Healing Ability

Waterborne polyurethanes bearing Diels–Alder bonds (PUDA) were synthesized by the acetone process by using a polyether polyol, i.e., poly(tetramethylene glycol), and different diisocyanate molecules, namely isophorone diisocyanate (IPDI), 4,4'-dicyclohexylmethane diisocyanate (HMDI), and

hexamethylene diisocyanate (HDI). The complete synthesis route is schematically reported in **Figure 1**.

First, an isocyanate-terminated prepolymer is obtained through the di-*n*-butyldilauritin (DBTDL)-catalyzed reaction between the polyol and the diisocyanate. In this step, 2,2-bis(hydroxymethyl)propionic acid (DMPA) is used as internal emulsifier. Then, a previously synthesized hydroxyl group functionalized molecule containing DA bonds is added to the reaction mixture. At the end of these first two reaction steps, an end-functionalized Diels–Alder pre-PU was obtained. Upon addition of hexamethylene diisocyanate trimer (Tri-HDI), interchain crosslinking takes place. At this stage, an excess of free DA molecules in the reaction mixture is necessary to endow the crosslinking points with dynamic ability. Besides being among the most commonly used commercially available ones, the selected diisocyanates significantly differ in terms of chemical structure, providing enough cues for studying the effect of the PU chemistry on the performances of the coatings. Indeed, the IPDI, HMDI and HDI molecules are characterized by a different degree of rigidity, symmetry, and reactivity.^[19] The resulting PUDA coatings are hence expected to possess different chain mobility, structural organization of the polymeric chains and extent of hydrogen bonding.

A first insight into the effect of the diisocyanate molecule on the chemical–physical properties of the PUDA was gained by Fourier transform infrared (FTIR) spectroscopy. The spectra of the different samples are compared in **Figure 2a**. In all the

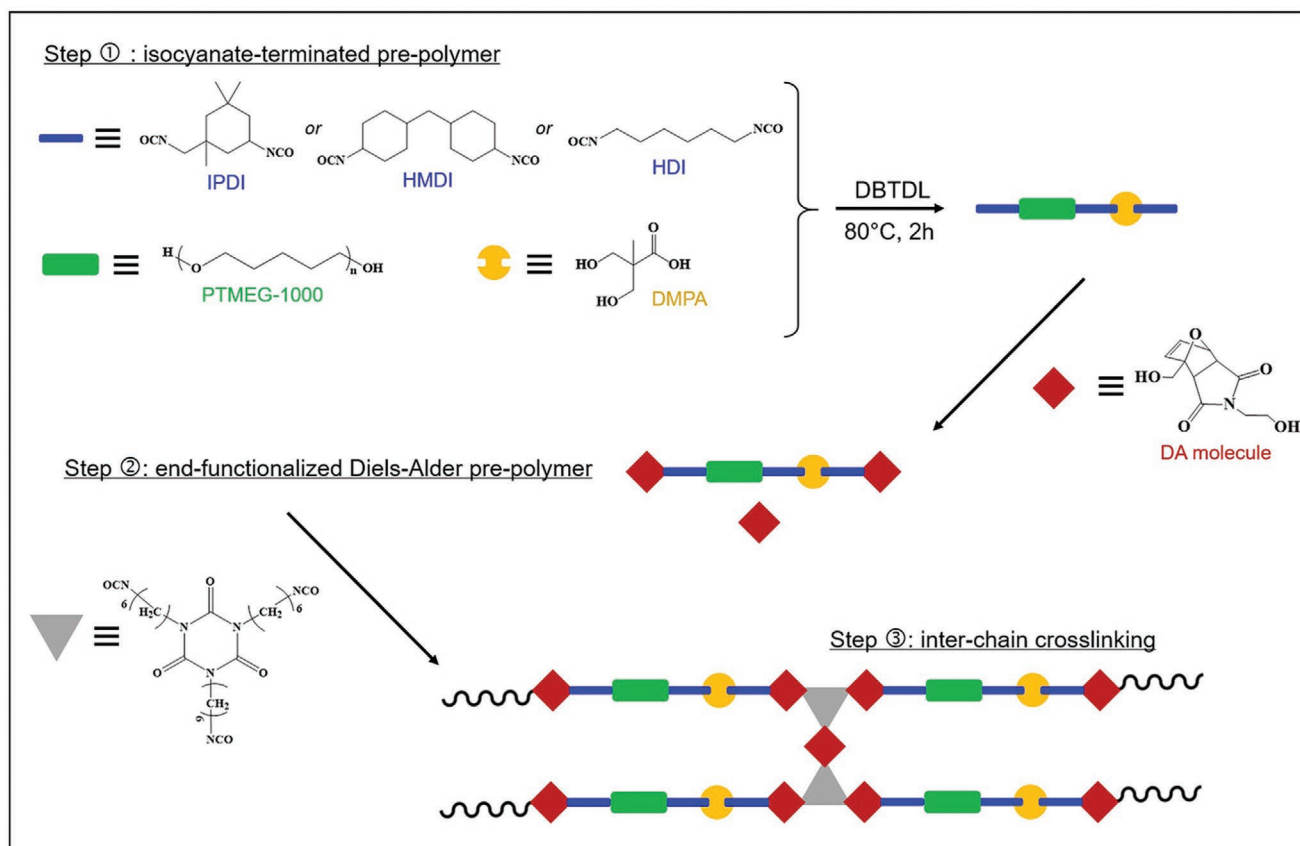


Figure 1. Reaction scheme of the PUDA synthesis.

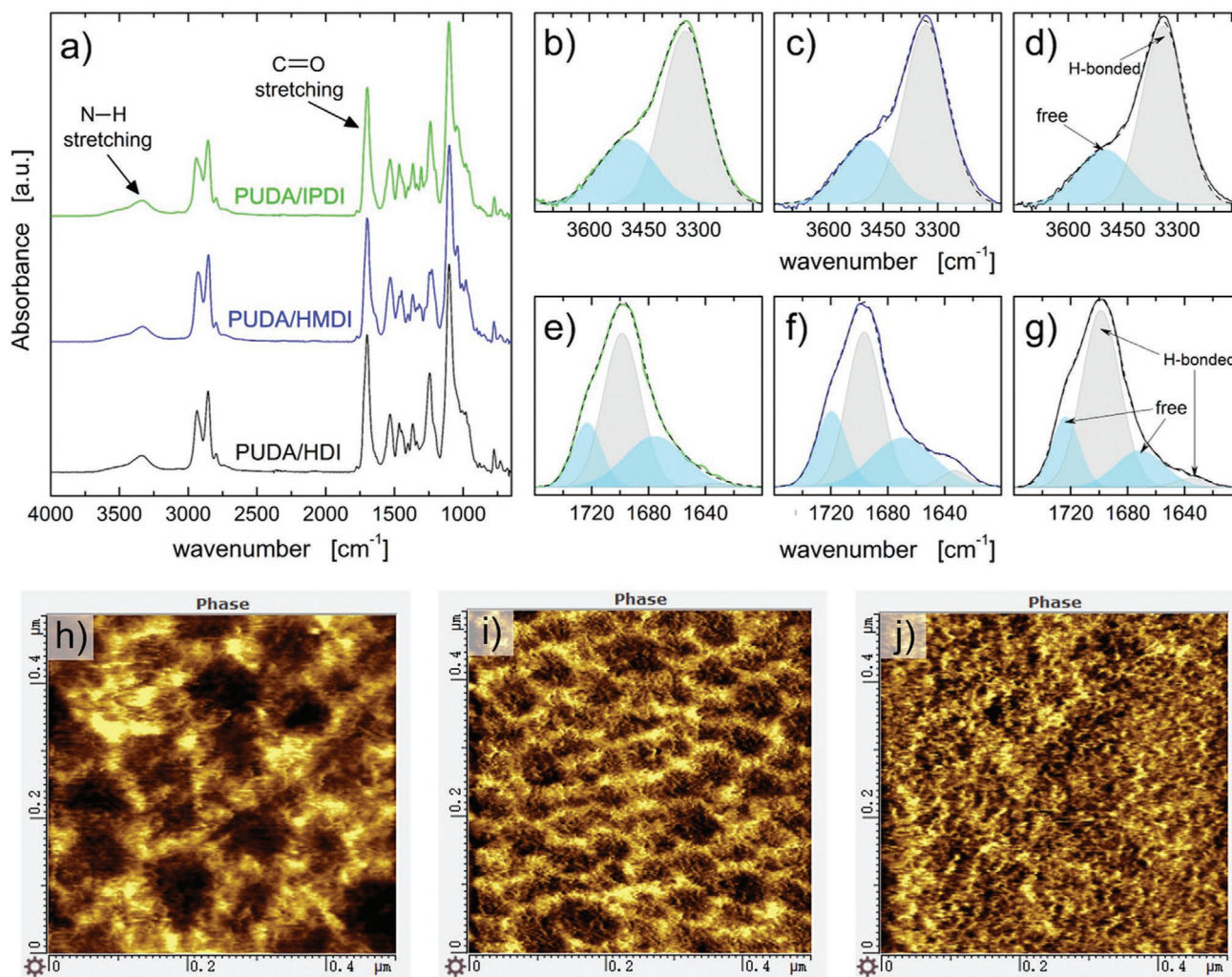


Figure 2. a) ATR-FTIR spectra of the synthesized PUDA films (spectra have been vertically shifted for the sake of clarity). Deconvoluted FTIR spectra in the b–d) N–H and e–g) C=O stretching regions: b,e) PUDA/IPDI, c,f) PUDA/HMDI, and d,g) PUDA/HDI. Solid and dashed lines correspond to the experimental and calculated spectrum, respectively. Deconvoluted peaks colored in light blue and gray correspond to free and hydrogen-bonded groups, respectively. AFM phase images of h) PUDA/IPDI, i) PUDA/HMDI, and j) PUDA/HDI systems.

investigated PUDA, the absence of the characteristic peak of the free —NCO group at about 2270 cm^{-1} indicates that the diisocyanate molecules completely reacted with the polyol.^[32]

In polyurethanes, hydrogen bonding between hard–hard and hard–soft segments plays a key role in dictating the final properties of the material. In particular, the NH group can form hard–hard segment H-bonding with the carbonyl oxygen, and hard–soft segment H-bonding with the ether oxygen (for polyether polyols).^[23,33,34] Peak deconvolution and best fit with a Gaussian–Lorentzian sum of FTIR spectra can be exploited to investigate the degree of hard and soft segment interaction. All the parameters obtained from the peak deconvolution and best fitting procedure are reported in Table S1 in the Supporting Information. In the N–H stretching region, the strong vibration band at about 3335 cm^{-1} can be assigned to H-bonded species, while the shoulder at higher frequency (around 3500 cm^{-1}) corresponds to free groups (Figure 2b–d). The peak area ratio reveals that most of the NH groups are hydrogen bonded, with

only small differences among the investigated systems: $\approx 68\%$, 70% , and 72% for the PUDA/IPDI, PUDA/HMDI, and PUDA/HDI coating, respectively. Concerning the carbonyl stretching region (Figure 2e–g), four different bands can be identified, belonging to free and H-bonded carbonyls from urethane and urea groups. More specifically, the peaks at around 1720 and 1699 cm^{-1} correspond to free and H-bonded C=O of the urethane group, while the peaks at around 1670 and 1635 cm^{-1} are related to free and H-bonded C=O of the urea group, respectively. The analysis of the H-bonded carbonyls allows to evaluate the extent of hard-hard segment interactions, and in turn also the complementary hard-soft ones. For this purpose, the hydrogen-bonding index (HBI), which is defined as the ratio between the total area of H-bonded carbonyls over that of free ones,^[35] can be calculated. The HBI value is a measure of the degree of interaction among hard segments, which can act as physical crosslinks and hinder segmental motion of the polymeric chains. The computed HBI values are ≈ 1.2 , 1.1 , and 1.9

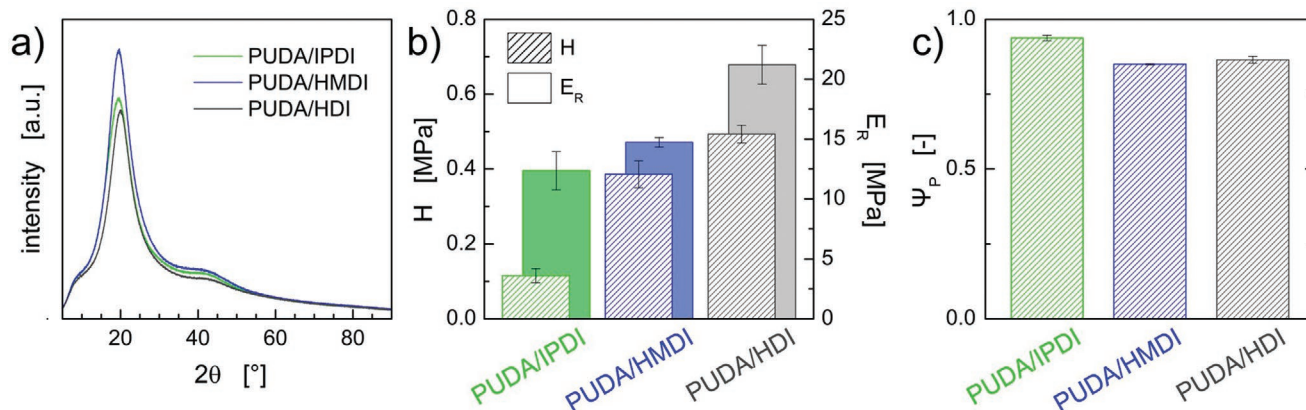


Figure 3. a) XRD patterns of the different PUDAs. b) Hardness and reduced elastic modulus and c) plasticity index obtained through nanoindentation measurements on PUDA-based coatings.

for the PUDA/IPDI, PUDA/HMDI, and PUDA/HDI coatings, respectively. Higher HBI values reflect extensive incompatibility between hard and soft segments, as can be appreciated by the degree of phase separation values reported in Table S2 in the Supporting Information.^[34] The higher degree of phase separation that characterizes the PUDA/HDI system is likely due to the linear, symmetrical, and planar structure of the HDI diisocyanate which facilitates the hard–hard segment interactions, eventually promoting phase separation.^[24] The phase morphology of PUDA-based formulations was also investigated by atomic force microscopy (AFM) (Figure 2h–l). The bright domains (i.e., hard segments) of PUDA/HDI are much smaller than that in the other systems, thus suggesting a more orderly microphase separation.^[36] On the other hand, the steric hindrance of the hexatomic rings of IPDI and HMDI molecules impeded the orderly stacking of the hard segments, which in turn better mixed into soft ones.^[37] X-ray diffraction (XRD) analyses were also performed to further study the morphology of the different polyurethanes (Figure 3a). All the PUDA samples exhibited a strong characteristic peak at $2\theta \approx 20^\circ$, corresponding to the crystallization of soft the segments.^[22,38] The significantly higher peak intensity of the PUDA/HMDI sample indicates that the cycloaliphatic diisocyanate favored the formation of more crystalline domains.^[39] The lower crystallinity in the IPDI-based polyurethane is not unexpected and it is mainly ascribable to the asymmetrical structure of the diisocyanate that destroyed the structural regularity of the soft segments.^[24,37] In the PUDA/HDI sample, instead, the strongly H-bonded hard segments hinder the molecular motion of soft segments chains inhibiting their crystallization.^[40]

The different phase morphology exhibited by the PUDA systems is also expected to bring about different mechanical properties. Although high hardness and reduced elastic modulus are necessary to ensure wear/scratch resistance, when dealing with self-healing coatings chain mobility is a prerequisite to fill the cracks and allow reactive groups to reassociate.

Nanoindentation tests, indeed, showed that the values of reduced elastic modulus, E_r , and hardness, H , of the PUDA/HMDI coating are in between those of PUDA/IPDI and PUDA/HDI ones (Figure 3b), suggesting that the balance between extent of H-bonding among hard segments and degree of

crystallization of the poly(tetramethylene glycol) chains in the soft segments results in a good tradeoff of mechanical properties. At the same time, all the investigated PUDA systems are characterized by a high value of the plasticity index, that is the ratio of the plastic work over the total work done during indentation and could be beneficial for allowing a fast and effective recovery during the healing process (Figure 3c).

The self-healing ability of the different PUDA-based systems was first investigated by monitoring the recovery of scratches of about 300 μm in width and 100 μm in depth during thermal treatment at 110 $^\circ\text{C}$ (Figure 4). After only 15 s, all the samples exhibited a significant degree of healing, which points out the key role of the Diels–Alder adduct in the PU backbone and crosslinking points. A PU sample without the DA component, indeed, was not able to recover the scratch upon heating (Figure S1, Supporting Information). The excellent self-healing ability of the PUDA systems is thus to be ascribed to the dissociation of DA bonds in main chains and crosslinked points, which tremendously improve the mobility of molecular chains. More in detail, the PUDA/HMDI formulation entirely repaired on a scratch length of over 3 mm, while small holes are still present on the surface of the other systems. In the healed regions, laser scanning confocal microscopy revealed that complete refilling of the scratched area is obtained for all the PUDA formulations (Figure S2, Supporting Information).

The self-healing temperature is mostly dependent on the chemistry behind the reversible bonds included in the formulation. For PUs based on Diels–Alder adducts, the temperature needed to promote the reversibility of the covalent bonds is often relatively high, otherwise poor mechanical properties are typically obtained at room temperature. For example, Du et al. obtained self-healing of a Diels–Alder-based polyurethane/urea from polymeric methylene diphenyl diisocyanate after thermal treatment at 130 $^\circ\text{C}$.^[41] The authors also showed that below 130 $^\circ\text{C}$ the self-healing process cannot be activated. Only very few studies, indeed, managed to combine good mechanical properties and self-healing ability at mild temperature.^[42] On the other hand, the kinetics of the self-healing process also has to be considered as a key point. While many self-healing systems necessitate of long thermal treatments in order to be fully repaired,^[43] for the PUDA-based systems the recovery of scratches is extremely fast.

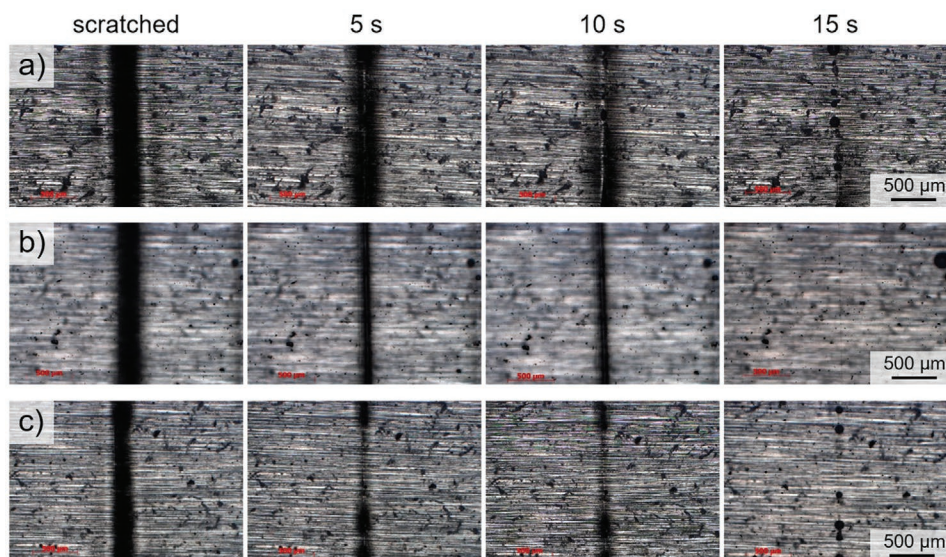


Figure 4. Optical micrographs of scratched PUUDA-based samples after thermal treatment of different duration: a) PUUDA-IPDI, b) PUUDA/HMDI, and c) PUUDA/HDI.

Depending on the coating thickness and scratch depth, the time needed to completely heal a damaged coating can be as low as tens of seconds, as shown in Figure 4.

2.2. Anticorrosion Properties

A first indication of the anticorrosion ability of the PUUDA-based formulations can be gained after exposing the coated bronze disks to an aggressive environment obtained by storing the coated disks in a drier containing a saturated solution of KCl. The high relative humidity ($\approx 85\%$) and high chloride species concentration are responsible of corrosion phenomena that specifically interest copper-based alloys, also known as “bronze disease,”^[44] which is a serious problem especially in the field of cultural heritage preservation.^[45] After about 5 months, the samples were collected and the metal surface was inspected by optical microscopy after gently removing the polymeric coating (Figure 5).

For all the samples, the disk surface is opaque and, in some cases, unevenly distributed large dark spots can be identified. Nonetheless, the metal surface is significantly less affected when protected by the PUUDA/HMDI coating (Figure 5c) than in the case of PUUDA/IPDI or PUUDA/HDI systems (Figure 5a,b, respectively). This is even more evident when looking at the optical micrographs, in which corrosion products can be clearly distinguished as black areas on the bronze surface.^[9,10,46–48]

The anticorrosion performances of the as-prepared PUUDA coating/bronze systems were also investigated by potentiodynamic polarization tests (Figure 6). With respect to the bare bronze disk, the polarization curves shifted in the positive direction for the potential and towards lower values of current density for all the coating formulations, thus indicating a good protective action. For a more quantitative comparison, the corrosion potential, E_{CORR} , and corrosion current density, I_{CORR} , values were calculated from the anodic and cathodic segment

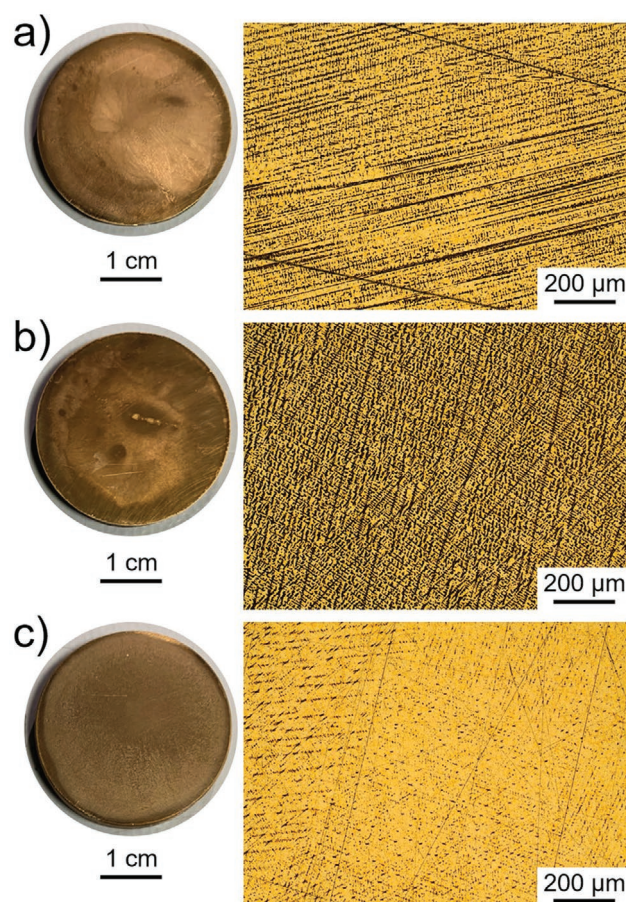


Figure 5. Pictures of disks after prolonged exposure to a corrosive environment and corresponding optical micrographs showing the appearance of the metal surface: a) PUUDA-IPDI, b) PUUDA/HDI, and c) PUUDA/HMDI.

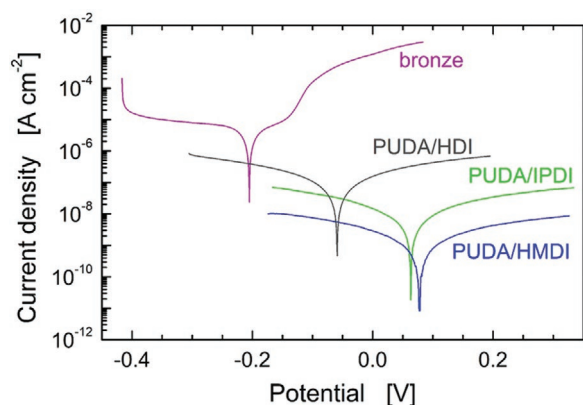


Figure 6. Potentiodynamic polarization curves of bare bronze and bronze disks coated with different PUHA systems.

of the polarization curves and are reported in Table S3 in the Supporting Information. The lowest I_{corr} value was found for the PUHA/HMDI coating, which hence ensures the lowest corrosion rate. The protective action of the PUHA/IPDI is also high, while inferior performances characterize the PUHA/HDI formulation. Overall, the protection efficiency, PE, of the

coatings has been calculated from the I_{corr} values,^[49] revealing an outstanding anticorrosion ability for the PUHA/HMDI and PUHA/IPDI systems (PE equal to 99.9% and 99.2%, respectively). On the contrary, the PUHA/HDI formulation exhibits a lower protection efficiency (PE \approx 85%).

To get a deeper insight into the anticorrosion properties of the PUHA-based coatings electrochemical impedance spectroscopy (EIS) analyses were also performed. The Bode plots of the different PUHA coating/bronze systems are reported in Figure 7.

A first screening has been performed by looking at the Bode plots after 30 min of contact with a 3.5 wt% NaCl solution (Figure 7a). In general, the value of the impedance modulus at low frequency can be taken as a qualitative indication of the coating barrier performances.^[50–52] Accordingly, the PUHA/HMDI coating exhibit the highest protective ability, while the PUHA/HDI one is characterized by poor anticorrosion performances, which is in line with the results of the potentiodynamic polarization tests. The difference in the protective ability is even more evident after 7 days, as shown in Figure 7b. Indeed, while the EIS spectra of the PUHA/IPDI and PUHA/HMDI coatings are relatively stable, the low-frequency behavior of the PUHA/HDI systems clearly indicates the failure of the barrier properties of the coating.

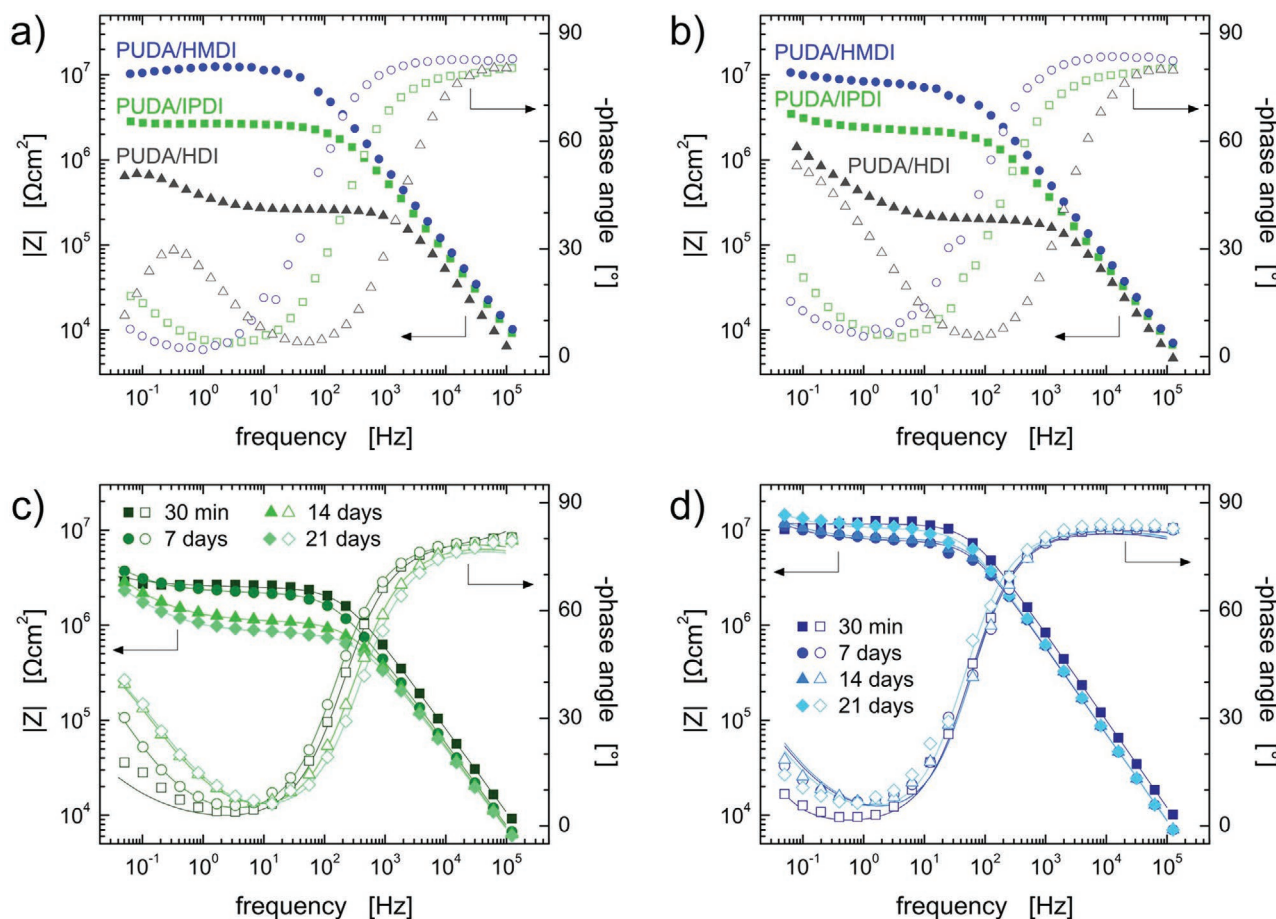


Figure 7. Bode plots for the different coating/bronze systems after a) 30 min and b) 7 days. Time evolution of the Bode plots over 21 days for c) PUHA/IPDI and d) PUHA/HMDI coatings on bronze. Symbols are experimental data (one out of three point is showed) and solid lines are the result of the fitting to the equivalent circuit model. In all plots, the impedance modulus is represented by full symbols (left-hand y-axis) and the phase angle by empty ones (right-hand y-axis).

Besides the inherent barrier properties of the coating, the adhesion to the underlying metal substrate is also considered a key requisite for ensuring a good anticorrosion efficacy. For the investigated systems, the adhesion on bronze was thus evaluated by crosscut tests (see Section S4, Supporting Information). An excellent adhesion to the bronze surface characterizes the PUDA/HMDI formulation. Differently, flaking along cut edges and partial coating detachment was observed for PUDA/IPDI and PUDA/HDI systems. Their similar adhesion properties thus cannot be considered a key factor to explain the marked differences in terms of anticorrosion performances that emerged from potentiodynamic polarization and EIS tests. In this sense, the worst protective ability of the PUDA/HDI formulation can be also ascribed to moisture trapped between the coating and metal surface during the drying process. For slow coating drying, indeed, corrosion phenomena can be prematurely initiated by water molecules present at the interface with the metal. The PUDA/HDI dispersion is characterized by smaller particles (see Section S5, Supporting Information), as it has been reported that relatively large particles are preferred in surface coatings for rapid drying.^[53] XRD measurements performed after different drying time support this picture, revealing that at relatively short times, i.e., one week, the crystallinity of the PUDA/HDI sample is far from that of a totally dried sample (Figure S5, Supporting Information). This issue can be in principle overcome by selecting more severe drying conditions, such as high temperatures or vacuum drying, but these strategies are not really feasible from a practical perspective. Accordingly, the PUDA/IPDI and PUDA/HMDI coatings clearly provide a more effective and reliable protection from corrosion, without requiring any specific expedient during coating deposition and/or drying. For this reason, their electrochemical behavior was further investigated by prolonging EIS experiments up to 21 days of immersion (Figure 7c,d). A first visual inspection of the spectra suggests that the PUDA/HMDI coating is quite stable over time, thus providing an effective barrier against aggressive species that may initiate corrosion processes. More quantitative information was gained by analyzing the EIS spectra with an equivalent circuit model, from which the coating properties can be evaluated (see Section S7, Supporting Information). Typically, the penetration of the electrolyte into a coating due to the failure of its barrier properties reflects in a decrease of the coating resistance, R_C , and an increase of the coating capacitance, Q_C , over time. This behavior clearly characterizes the PUDA/IPDI coating, whose resistance drops upon exposure to the NaCl solution. At the same time, the Q_C value constantly increases over time, indicating the formation of a continuous and percolated defective path within the polymeric layer that can host growing amounts of electrolyte. On the contrary, the R_C of the PUDA/HMDI sample only slightly decreases during the first days, and then reaches an almost constant value. Notably, the coating resistance of the PUDA/HMDI system is even higher of that of other waterborne coatings in which nanocontainers and corrosion inhibitor molecules have been added to improve the protective performances.^[52,54] The coating capacitance exhibits a specular behavior, as it rapidly gets to a time-independent value after few days. The plateauing of the electrochemical parameters that characterize the response of the PUDA/HMDI coating strongly evidences its protective ability.

According to all the previous results, the PUDA/HMDI sample stands out as the most promising protective anticorrosion coating. Nonetheless, the strong adhesion to the bronze substrate (see Section S4, Supporting Information) may in turn negatively influence the self-healing ability of the PUDA/HMDI system once it is applied in the form of a coating because of chain adsorption on the metal substrate and consequent mobility reduction. As a result, extending the results obtained on films (Figure 4) to thin coatings with thickness of tens of micrometers is not straightforward. For this reason, additional self-healing experiments were also performed on coatings (Figure 8a).

Although the time needed to complete the healing of the damage is slightly longer than for bulk samples, the images before and after the thermal treatment prove that the PUDA/HMDI formulation can still quickly and efficiently recover even in the form of few-micrometer-thick coating. In the light of these results, additional tests were performed to correlate the coating self-healing ability with the recovery of its protective features. To this aim, a scratch (about 100 μm in width and 2 cm in length) was made through the PUDA/HMDI coating to the surface of the bronze disk by a razor blade. After a thermal treatment at 110 °C for 5 min in an air-circulating oven to promote healing, the recovery of the coating anticorrosion ability was investigated by EIS measurements. As expected, the scratched coating is characterized by a significant lowering of the impedance modulus after being exposed to the electrolyte solutions for only 30 min, which suggest the complete loss its protection ability (Figure 8b). Differently, the scratched and then thermally healed coating fully recovers its barrier properties, as emerges from the comparison with the behavior of an as-prepared PUDA/HMDI sample. Moreover, the anticorrosion ability of the healed coating is also stable over time, as indicated by the EIS tests performed after 21 days (Figure 8c).

3. Conclusions

The role of the diisocyanate molecule in determining the anticorrosion and self-healing properties of polyurethane-based coatings was systematically investigated. Waterborne polyurethanes were synthesized according to the acetone procedure by using a polyether polyol (PTMEG-1000), and different diisocyanate molecules, namely isophorone diisocyanate, 4,4'-dicyclohexyl methane diisocyanate, and hexamethylene diisocyanate. A previously synthesized Diels–Alder adduct was also inserted into the backbone and crosslinking points to endow the polymer with self-healing ability. The different nature of the selected diisocyanates resulted in polyurethane coatings characterized by significantly different properties. In particular, FTIR analyses showed that the PUDA/HMDI system is characterized by strong H-bonding among hard segments, yet exhibiting the lower degree of phase separation between hard and soft segments with respect to the other PUDA formulations. This brings about a higher crystallization ability of the soft segments, as proved by XRD spectra. The balance between hard–hard segments interactions and soft segments crystallinity endows the PUDA/HMDI coating with a good mechanical properties and excellent anticorrosion ability. Despite the

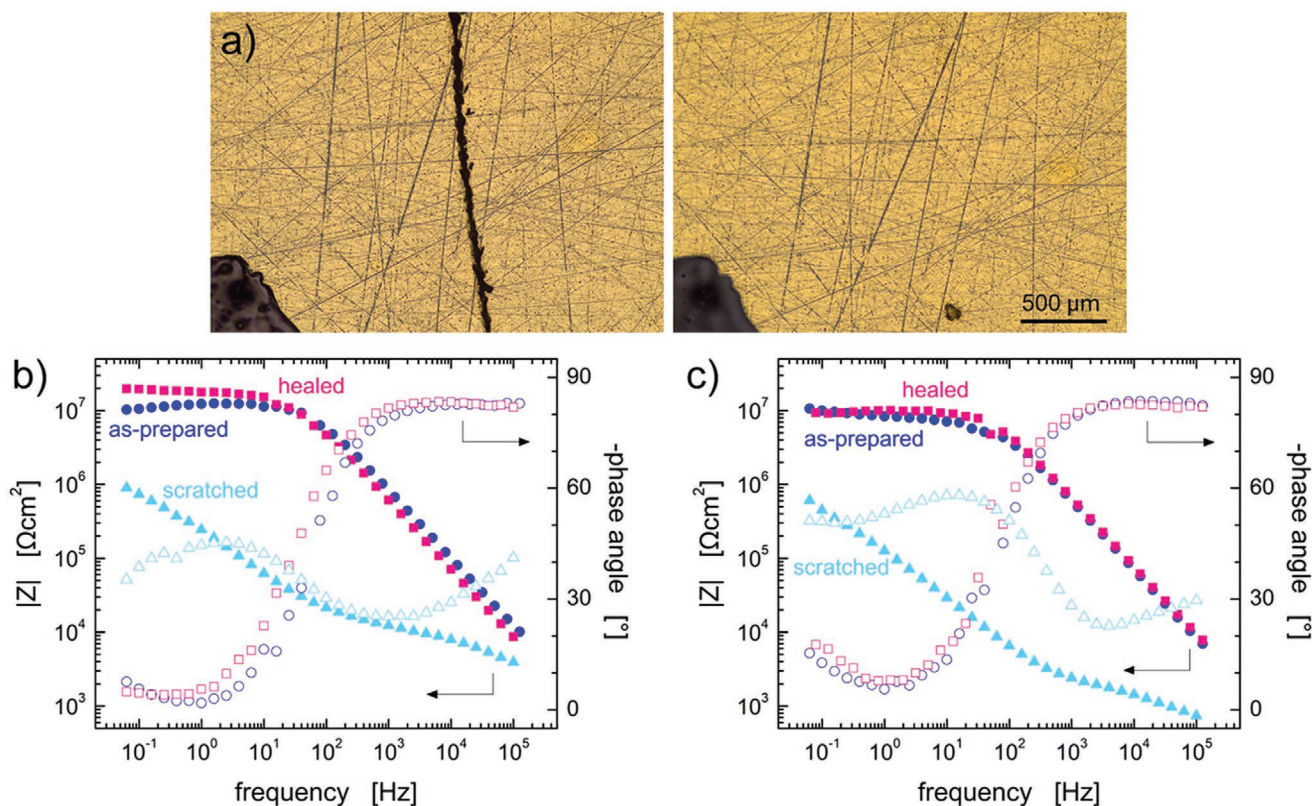


Figure 8. a) Optical micrographs of scratched PU/DA/HMDI coating (50 μm thick) before (left) and after (right) thermal treatment at 110 $^{\circ}\text{C}$ for 5 min. The black spot on the bottom-left of the image serves as reference for the scratched area. b,c) Bode plots for the as-prepared, scratched, and healed PU/DA/HMDI coatings on bronze disks after b) 30 min and c) 21 days. The impedance modulus is represented by full symbols (left-hand y-axis) and the phase angle by empty ones (right-hand y-axis). Only one out of three points is showed.

chain rigidity and high barrier properties that are required for protective purposes, the PU/DA/HMDI sample also possess enough chain mobility to allow the complete recovery of deep scratches after only few seconds of heat exposure.

4. Experimental Section

Preparation of PU/DA Coatings: The self-healing waterborne polyurethanes were synthesized according to the following procedure, which is also schematically reported in Figure 1. PTMEG-1000 (10 mmol), diisocyanate (HMDI or IPDI or HDI, 20 mmol), and DMPA (4.17 mmol) were added into single-port flask equipped with a condenser and stirred to react at 80 $^{\circ}\text{C}$ for 2 h. PTMEG-1000 was kept at 120 $^{\circ}\text{C}$ under vacuum for 2 h before using to remove moisture. One drop of DBTDL and acetone (15 mL) were then added to the reaction flask under stirring. DA molecules (8.34 mmol), previously synthesized following the approach introduced by Lu et al.,^[28] were added and keep reacting at 80 $^{\circ}\text{C}$ for 2 h. Then Tri-HDI (1.67 mmol) was added to crosslink the molecular chains. After reacting for another 2 h, the temperature was lowered to 40 $^{\circ}\text{C}$ and triethylamine (580 μL) was added to completely neutralize DMPA. In 20 min, the solution was poured into a vial and emulsified at 6000 rpm (Ultra-Turrax T25 digital, IKA). Acetone was removed by rotary evaporator at 40 $^{\circ}\text{C}$ and the self-healing waterborne polyurethane dispersion was obtained. Finally, the coatings were obtained by drop casting proper amounts of the PU/DA dispersion (≈ 36 wt% of polymer) on bronze disks previously polished and cleaned with ethanol.

Characterization: FTIR spectroscopy was carried out in attenuated total reflectance (ATR) mode with a Perkin Elmer Spectrum One

spectrometer. The ATR spectra were recorded at a resolution of 4 cm^{-1} and 64 scan collections on 50 μm thick coatings deposited on glass slides. Baseline correction was applied to the reported spectra. AFM with a SmartSPM equipment (AIST-NT, America) in tapping mode was used to investigate the phase morphology of the PU/DA-based systems. To this aim, PU/DA emulsions were diluted to 1 wt%, then dropped onto mica plates and dried at room temperature. The results were analyzed by Testdb software to obtained AFM phase images (0.5 $\mu\text{m} \times 0.5 \mu\text{m}$). X-ray diffraction analyses were performed with an X-ray diffractometer (Empyrean) equipped with a $\text{Cu-K}\alpha$ source and operating at 40 kV and 40 mA in the 2θ range of 5 $^{\circ}$ –80 $^{\circ}$. The tested samples were prepared by dropping 1 mL emulsion onto a Teflon film and dried at room temperature. Nanoindentation experiments were carried out with a NanoTest Platform (Micro Materials Ltd) equipped with a standard three-sided pyramidal Berkovich probe. The tests were performed with a loading rate of 0.1 mN s^{-1} and a holding time of 60 s at the maximum load during before unloading. The penetration depth was kept within 10% of the sample thickness to avoid interference of the substrate.^[55] Ten loading–unloading curves were recorded for each sample, from which the hardness and reduced elastic modulus were determined according to the Oliver and Pharr method,^[56] and the plasticity index was also estimated to assess the relative plastic/elastic character of the coating material.^[57] The self-healing ability of the coatings was assessed by monitoring the time recovery of scratches made by razor blades after subjecting the samples to thermal treatments at 110 $^{\circ}\text{C}$. Optical and laser scanning confocal microscopy were exploited to image the scratched area. The anticorrosion ability of the different formulations was assessed after storing the coated disks at room temperature in a drier containing a saturated solution of KCl, thus keeping the relative humidity value to about 85%. More

quantitative information was also gained through potentiodynamic polarization analyses and electrochemical impedance spectroscopy, which were both exploited to investigate the ability of the coatings to protect the underlying metal surface from corrosion. The experiments were carried out by using a Biologic SP150 potentiostat with a fully aerated 3.5 wt% NaCl aqueous solution at room temperature and neutral pH. Potentiodynamic polarization curves were obtained by a scanning the potential at scan rate of 0.3 mV s⁻¹ in the range from -250 to +250 mV with respect to the open circuit potential value. Electrochemical impedance spectroscopy was carried out with a two-electrode configuration, in which the working electrode was the coated bronze disk, in potentiostatic mode at open circuit potential. The spectra have been collected over time, up to 21 d. EIS measurements were performed on as-prepared coated disks to assess the different anticorrosion efficacy of the PUDA-based formulations. At the same time, to appreciate the self-healing ability, EIS test were also carried out on scratched and healed coatings.

Supporting Information

Supporting Information is available from the Wiley Online Library or from the author.

Acknowledgements

C.Y. and M.S.d.L. contributed equally to this work. The “National Key Research and Development Program of China (2017YFE0111500)” Project, the International Cooperation Project of Sichuan Province (2019YFH0135), and “European Union Horizon 2020 Research and Innovation programme (No. 734164)” are acknowledged for financial support. The authors also thank Alessandra Aldi, Mario De Angioletti, and Fabio Docimo for the technical support in the experiments.

Conflict of Interest

The authors declare no conflict of interest.

Data Availability Statement

The data that support the findings of this study are available from the corresponding author upon reasonable request.

Keywords

coatings, corrosion protection, Diels–Alder, polyurethane, self-healing properties

Received: January 25, 2021

Revised: March 2, 2021

Published online: March 18, 2021

- [1] M. Cui, B. Wang, Z. Wang, *Adv. Eng. Mater.* **2019**, *21*, 1801379.
 [2] S. Liang, N. M. Neisius, S. Gaan, *Prog. Org. Coat.* **2013**, *76*, 1642.
 [3] W. Teng, N. Bai, J. Fan, D. Li, R. Liu, J. Yang, W. X. Zhang, D. Zhao, *RSC Adv.* **2016**, *6*, 81477.
 [4] H. Megahd, P. Lova, D. Comoretto, *Adv. Funct. Mater.* **2020**, *31*, 2009626.

- [5] H. Megahd, C. Oldani, S. Radice, A. Lanfranchi, M. Patrini, P. Lova, D. Comoretto, *Adv. Opt. Mater.* **2021**, *9*, 2002006.
 [6] P. Lova, H. Megahd, D. Comoretto, *ACS Appl. Polym. Mater.* **2020**, *2*, 563.
 [7] S. B. Lyon, R. Bingham, D. J. Mills, *Prog. Org. Coatings* **2017**, *102*, 2.
 [8] J. V. Nardeli, C. S. Fugivara, M. Taryba, E. R. P. Pinto, M. F. Montemor, A. V. Benedetti, *Prog. Org. Coat.* **2019**, *135*, 368.
 [9] C. Giuliani, M. Pascucci, C. Riccucci, E. Messina, M. Salzano de Luna, M. Lavorgna, G. M. Ingo, G. Di Carlo, *Prog. Org. Coat.* **2018**, *122*, 138.
 [10] M. Salzano de Luna, G. G. Buonocore, C. Giuliani, E. Messina, G. Di Carlo, M. Lavorgna, L. Ambrosio, G. M. Ingo, *Angew. Chem., Int. Ed.* **2018**, *57*, 7380.
 [11] A. A. Javidparvar, R. Naderi, B. Ramezanzadeh, *J. Hazard. Mater.* **2020**, *389*, 122135.
 [12] S. H. Cho, S. R. White, P. V. Braun, *Adv. Mater.* **2009**, *21*, 645.
 [13] T. Chang, F. Panhwar, G. Zhao, *Adv. Mater. Interfaces* **2020**, *7*, 1901959.
 [14] G. L. Li, M. Schenderlein, Y. Men, H. Möhwald, D. G. Shchukin, *Adv. Mater. Interfaces* **2014**, *1*, 1300019.
 [15] C. Zhu, Y. Fu, C. Liu, Y. Liu, L. Hu, J. Liu, I. Bello, H. Li, N. Liu, S. Guo, H. Huang, Y. Lifshitz, S. T. Lee, Z. Kang, *Adv. Mater.* **2017**, *29*, 1701399.
 [16] J. H. Xu, S. Ye, C. Di Ding, L. H. Tan, J. J. Fu, *J. Mater. Chem. A* **2018**, *6*, 5887.
 [17] J. O. Akindoyo, M. D. H. Beg, S. Ghazali, M. R. Islam, N. Jeyaratnam, A. R. Yuvaraj, *RSC Adv.* **2016**, *6*, 114453.
 [18] D. K. Chattopadhyay, K. V. S. N. Raju, *Prog. Polym. Sci.* **2007**, *32*, 352.
 [19] B. Willocq, J. Odent, P. Dubois, J.-M. Raquez, *RSC Adv.* **2020**, *10*, 13766.
 [20] Z. Liu, L. Zhang, Q. Guan, Y. Guo, J. Lou, D. Lei, S. Wang, S. Chen, L. Sun, H. Xuan, E. M. Jeffries, C. He, F. L. Qing, Z. You, *Adv. Funct. Mater.* **2019**, *29*, 1901058.
 [21] Y. Li, T. Hu, B. Li, J. Wei, J. Zhang, *Adv. Mater. Interfaces* **2019**, *6*, 1901255.
 [22] S. Y. Kang, Z. Ji, L. F. Tseng, S. A. Turner, D. A. Villanueva, R. Johnson, A. Albano, R. Langer, *Adv. Mater.* **2018**, *30*, 1706237.
 [23] S. M. Kakić, I. S. Ristić, M. Marinović-Cincović, M. Špirková, *Int. J. Adhes. Adhes.* **2013**, *41*, 132.
 [24] A. W. Grzelak, P. Boinard, J. J. Liggat, *Prog. Org. Coat.* **2018**, *122*, 1.
 [25] M. Špirková, J. Hodan, J. Kredatusová, R. Poręba, M. Uchman, M. Serkis-Rodzeń, *Prog. Org. Coat.* **2018**, *123*, 53.
 [26] W. T. Lin, W. J. Lee, *Colloids Surf., A* **2017**, *522*, 453.
 [27] S. Li, Z. Liu, L. Hou, Y. Chen, T. Xu, *Prog. Org. Coat.* **2020**, *141*, 105545.
 [28] X. Lu, G. Fei, H. Xia, Y. Zhao, *J. Mater. Chem. A* **2014**, *2*, 16051.
 [29] Z. Wang, X. Lu, S. Sun, C. Yu, H. Xia, *J. Mater. Chem. B* **2019**, *7*, 4876.
 [30] D. Fu, W. Pu, Z. Wang, X. Lu, S. Sun, C. Yu, H. Xia, *J. Mater. Chem. A* **2018**, *6*, 18154.
 [31] L. Tian, L. Yang, Z. Wang, H. Xia, *Acta Polym. Sin.* **2019**, *50*, 527.
 [32] E. Princi, S. Vicini, K. Castro, D. Capitani, N. Proietti, L. Mannina, *Macromol. Chem. Phys.* **2009**, *210*, 879.
 [33] E. Ayres, R. L. Oréfice, M. I. Yoshida, *Eur. Polym. J.* **2007**, *43*, 3510.
 [34] M. Aurilia, F. Piscitelli, L. Sorrentino, M. Lavorgna, S. Iannace, *Eur. Polym. J.* **2011**, *47*, 925.
 [35] R. W. Seymour, G. M. Estes, S. L. Cooper, *Macromolecules* **1970**, *3*, 579.
 [36] P. Du, X. Liu, Z. Zheng, X. Wang, T. Joncheray, Y. Zhang, *RSC Adv.* **2013**, *3*, 15475.
 [37] H. Fu, K. Liu, C. Yan, W. Chen, Y. Wang, *Polym. Polym. Compos.* **2015**, *23*, 141.
 [38] C. Tao, J. Bao, Q. Cheng, Y. Huang, G. Xu, *J. Adhes.* **2019**, *95*, 814.
 [39] K. M. Zia, I. A. Bhatti, M. Barikani, M. Zuber, M. A. Sheikh, *Int. J. Biol. Macromol.* **2008**, *43*, 136.
 [40] S. Mondal, J. L. Hu, *Polym. Eng. Sci.* **2008**, *48*, 233.

- [41] P. Du, M. Wu, X. Liu, Z. Zheng, X. Wang, T. Joncheray, Y. Zhang, *J. Appl. Polym. Sci.* **2014**, *131*, 40234.
- [42] T. T. Truong, S. H. Thai, H. T. Nguyen, D. T. T. Phung, L. T. Nguyen, H. Q. Pham, L. T. T. Nguyen, *Chem. Mater.* **2019**, *31*, 2347.
- [43] N. Babaei, H. Yeganeh, R. Gharibi, *Eur. Polym. J.* **2019**, *112*, 636.
- [44] D. A. Scott, *J. Am. Inst. Conserv.* **1990**, *29*, 193.
- [45] M. C. Bernard, S. Joiret, *Electrochim. Acta* **2009**, *54*, 5199.
- [46] M. Mihelčič, M. Gaberšček, G. Di Carlo, C. Giuliani, M. Salzano de Luna, M. Lavorgna, A. K. Surca, *Appl. Surf. Sci.* **2019**, *467–468*, 912.
- [47] M. Mihelčič, M. Gaberšček, M. Salzano de Luna, M. Lavorgna, C. Giuliani, G. Di Carlo, A. K. Surca, *Mater. Des.* **2019**, *178*, 107860.
- [48] R. Castaldo, M. S. de Luna, C. Siviello, G. Gentile, M. Lavorgna, E. Amendola, M. Cocca, *J. Cult. Heritage* **2020**, *44*, 317.
- [49] Y. Li, B. Li, X. Zhao, N. Tian, J. Zhang, *ACS Appl. Mater. Interfaces* **2018**, *10*, 39391.
- [50] B. R. Hinderliter, S. G. Croll, D. E. Tallman, Q. Su, G. P. Bierwagen, *Electrochim. Acta* **2006**, *51*, 4505.
- [51] Q. Mo, W. Li, H. Yang, F. Gu, Q. Chen, R. Yang, *Prog. Org. Coat.* **2019**, *136*, 105213.
- [52] Y. Wu, J. Yu, W. Zhao, C. Wang, B. Wu, G. Lu, *Prog. Org. Coat.* **2019**, *133*, 8.
- [53] M. M. Rahman, H. Do Kim, *J. Appl. Polym. Sci.* **2006**, *102*, 5684.
- [54] X. Liu, C. Gu, Z. Wen, B. Hou, *Prog. Org. Coat.* **2018**, *115*, 195.
- [55] K. Geng, F. Yang, T. Druffel, E. A. Grulke, *Polymer* **2005**, *46*, 11768.
- [56] W. C. Oliver, G. M. Pharr, *J. Mater. Res.* **1992**, *7*, 1564.
- [57] B. J. Briscoe, L. Fiori, E. Pelillo, *J. Phys. D: Appl. Phys.* **1998**, *31*, 2395.